Supporting Information

Spinneret as the key component for surface-porous graphene fibers in high energy density micro-supercapacitors

Table S1

Comparison of our micro-SC based on SGFs with other fiber supercapacitors reported previously.

Ref.	Materials	C_L(mFcm^{-1})	C_A(mFcm^{-2})	E_A(μWhcm^{-2})	C_V(Fcm^{-3})	E_V(mWhcm^{-3})
*	SGF(This work)	2.85	228	7.9	114.5	4.0
[1]	CNT/Carbon nanofiber	5.1	86.8	9.8		0.14
[2]	CNT sheet/CNT	0.029	8.66			
[3]	CNT/OMC	1.91	39.7	1.77		
[4]	CNT/MnO$_2$	0.015	3.7			1.73
[5]	CNT/PANI		38			
[6]	MWCNT/ PEDOT	0.47	73			1.4
[7]	Graphene		1.7	0.17		
[8]	ERGO	0.01	6.49			
[9]	Pen ink	1.008	26.4	2.7		
[10]	Carbon/MnO$_2$				2.5	0.22
[11]	MnO$_2$/ZnO	0.04	2.4	0.027		
[12]	PANI/SSS		41	0.95		
[13]	Porous carbon					0.37
[14]	CNT	0.24	52.5			
[15]	Graphene/CNT	0.027	4.97			
[16]	Graphene /MnO$_2$	0.14	9.6			
[17]	Graphene/Bi$_2$O$_3$		17.3			

CNT: carbon nanotube; MWCNT: multi-wall carbon nanotube; OMC: ordered mesoporous carbon;

PANI: polyaniline; PEDOT: poly (3,4-ethylenedioxythiophene); ERGO: electrochemical reduced

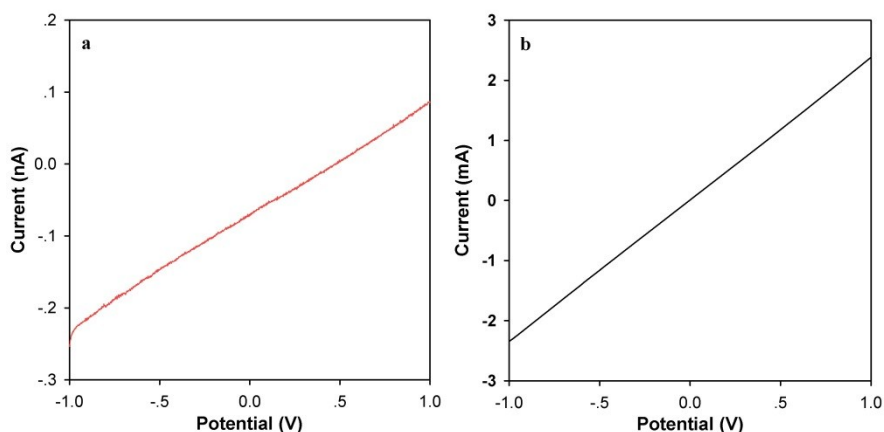graphene oxide. SSS: stainless steel.

Figure S1 (a) and (b) show the I–V curves of SGOFs and SGFs, respectively.

Electrical measurements (I–V curves) were also carried out on a CHI660E electrochemical workstation (using a two-electrode setup) by measuring the current produced at different voltages (from -1.0 to 1.0 V) with a potentiostatic technique [18]. Conductivity values were calculated from the slopes of the I–V curves and the diameter of each fiber which was measured using the SEM.
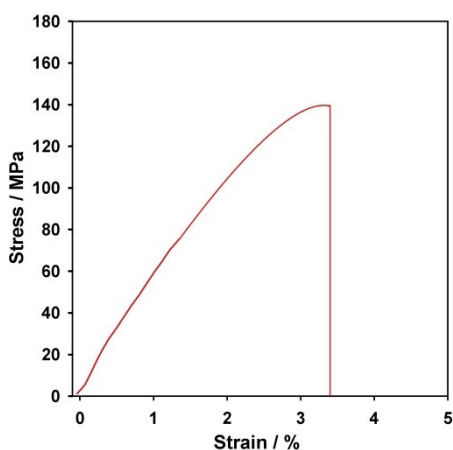

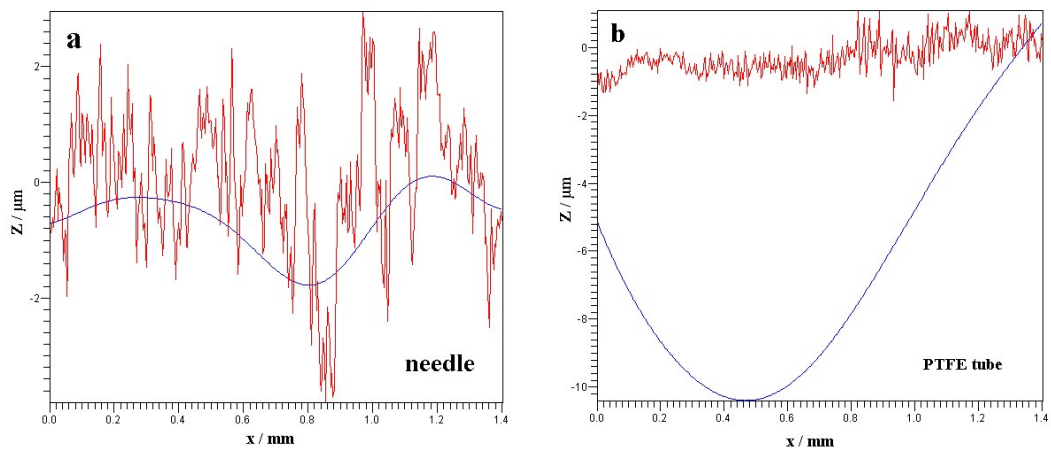Figure S2 Stress-strain curve of the SGF.

Figure S3. 3 Dimensional Surface Profilometer of the metal needle from a medical syringe (a) and the PTFE tube (b).
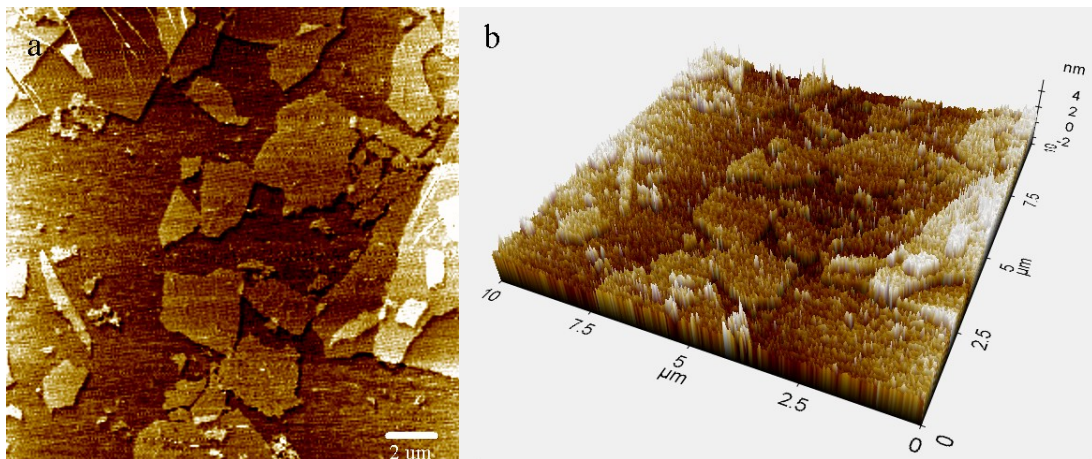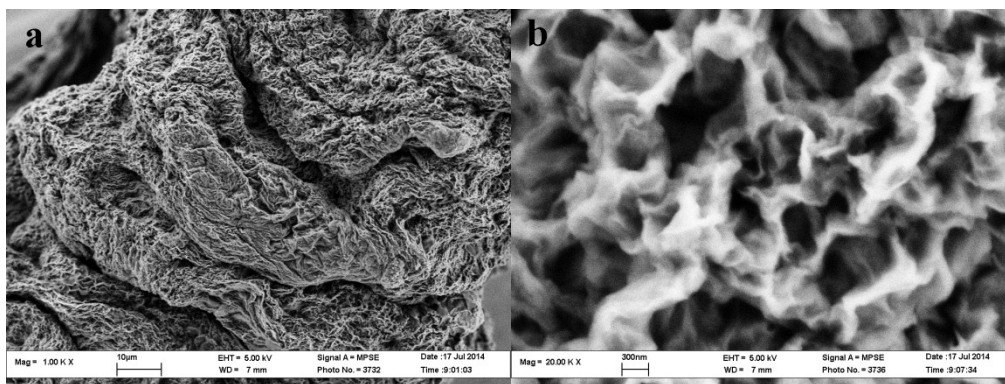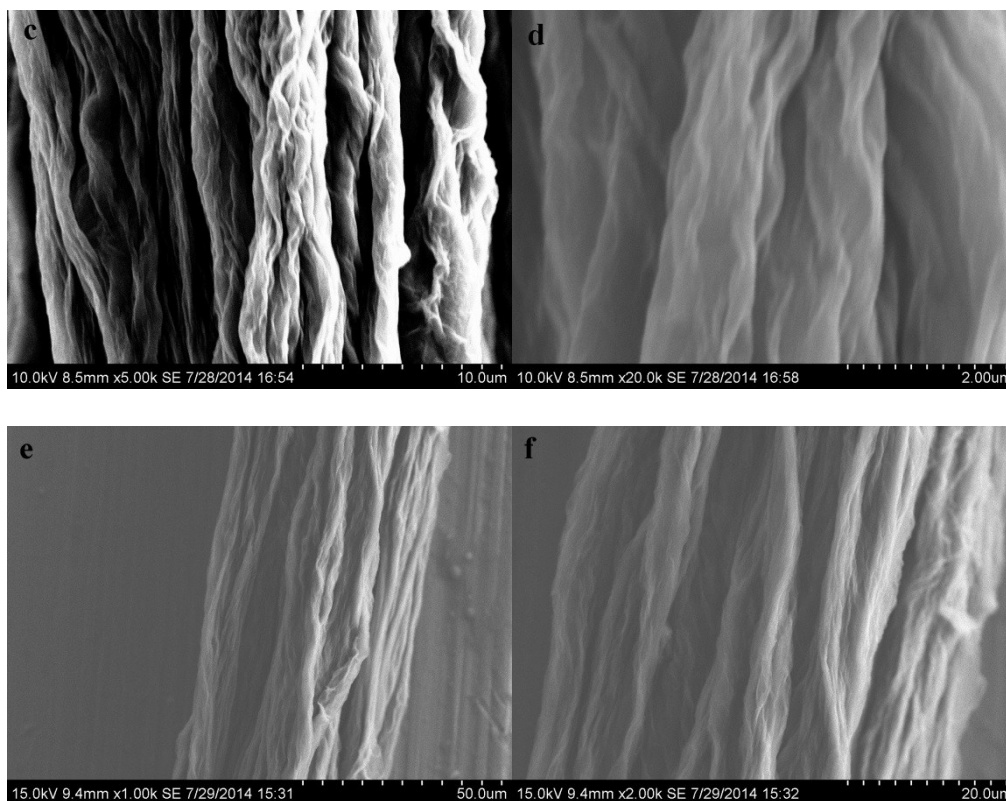

Figure S4. (a-b) AFM images of GO.

Figure S5 SEM images of the neat GO fibers including SGOFs (a,b); PGOFs (c,d) and the neat GO fibers obtained by using a glass capillary tube as the spinneret (denoted as GCGFs).

It could be clearly seen from the above SEM images that different kinds of spinnerets resulting in different shaped neat graphene fibers. When comparing with the PGOFs or GCGFs, the SGOFs possess lots of highly porous nanoscale sheets that probably lead to high-performance micro-SCs based SGFs.
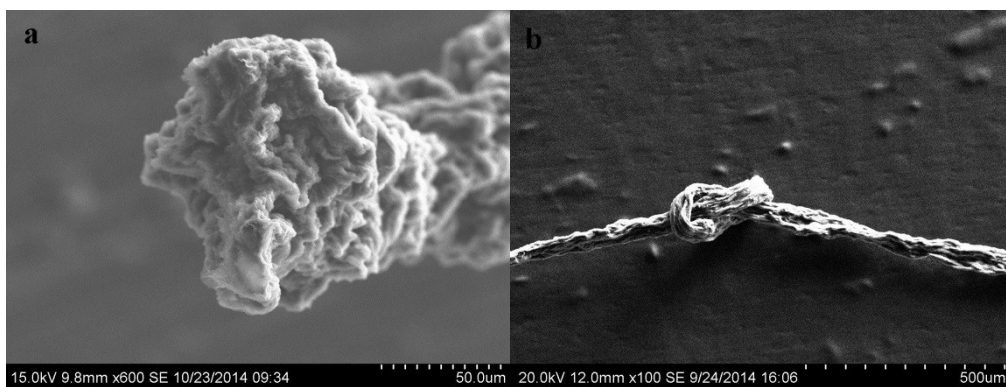
Figure S6 SEM images of the cross-section of a neat graphene fiber and the neat graphene fiber being made into a knot.
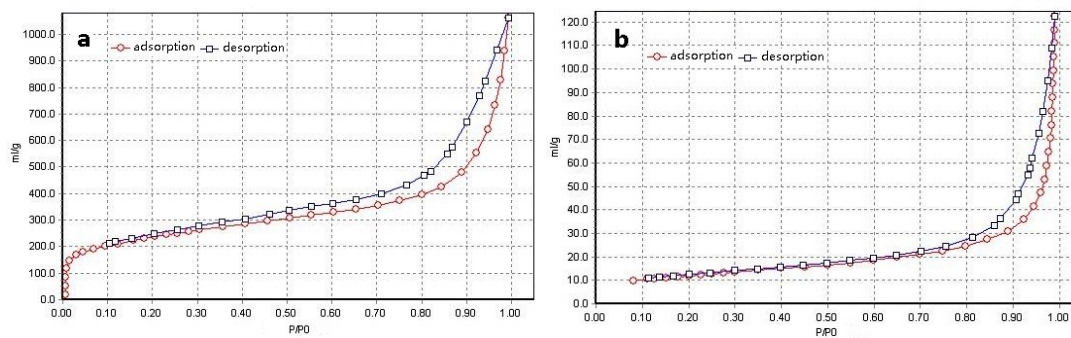

Figure S7 Nitrogen adsorption and desorption isotherm of the (a) SGF and (b) PGF.

Brunauere-Emmette-Teller (BET) specific surface area was obtained from the N_2 adsorption/desorption isotherm recorded at 77 K. The BET specific area of the SGF was calculated to be 815 m^2/g (Figure S7a), much larger than that of PGF (42 m^2/g, Figure S7b) from the nitrogen adsorption-desorption isotherm.
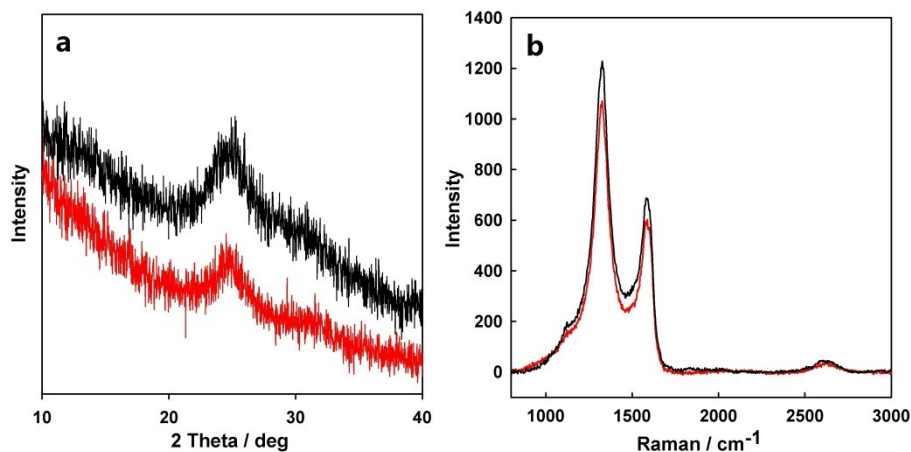
Figure S8 (a) X-ray diffraction (XRD) patterns of the SGF (red curve) and PGF (black curve); (b) Raman spectrum of the SGF (red curve) and PGF (black curve).

The as-prepared graphene fibers were characterized by X-ray diffraction (XRD). Both of the SGF (red curve) and PGF (black curve) showed almost the same diffraction peaks at $2\theta = 24.8°$ in the XRD patterns, indicating that there were no obvious differences in the crystal structure between SGF and PGF.

In the Raman spectrum, the SGF and PGF showed similar sharped peaks located at 1325 cm^{-1} for D band and 1581cm^{-1} for G band, which were characteristic peaks of graphene fibers as previous report [19]. Furthermore, both of the SGF and PGF showed the same I_D/I_G rate of 1.78, confirming that there no difference between the interior structure of the SGF and PGF.
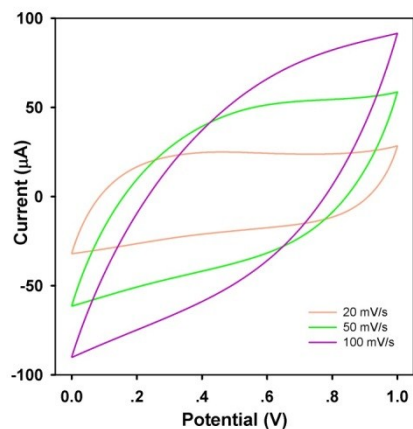
Figure S9 CV curves of the micro-SCs based on SGFs at high scan rates from 20 mV·s^{-1} to 100 mV·s^{-1}.
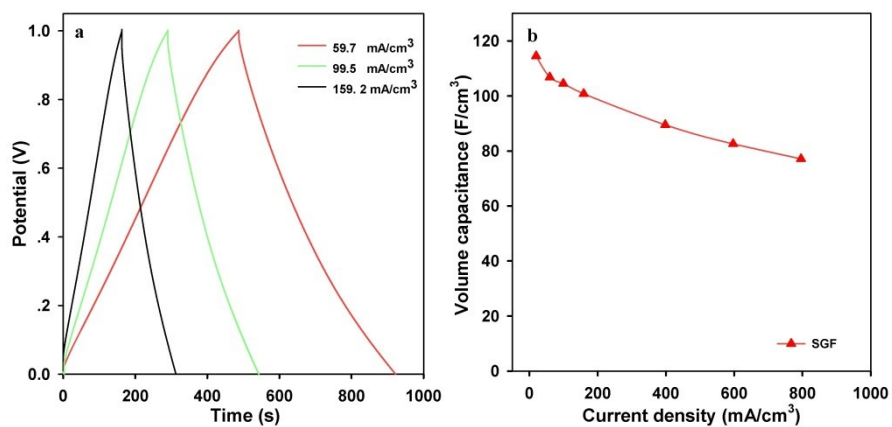

Figure S10 CC curves of a micro-SC based on SGFs (a) and the corresponding volumetric specific capacitance of a SGFs' electrode (b).

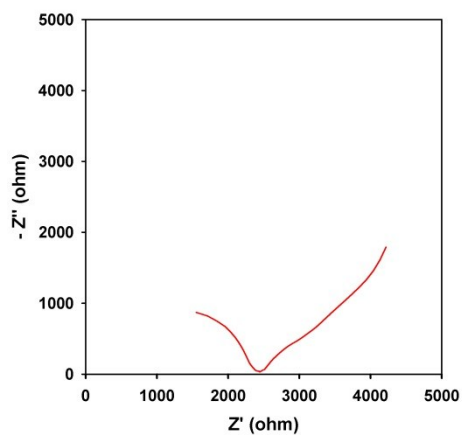Figure S11 Nyquist plot of the impedance of the SGFs (1 cm) in 1.0 M H$_2$SO$_4$ aqueous solutions.

Figure S11 shows that the SGFs still have relatively high impedance though they were already treated by 40% HI solutions. Further improvement on reducing the impedance of SGFs is under research in our lab.

Figure S12 A photograph of a metal needle with one sharped end (left) and the other flat end (right).

Measurement of the specific surface area of SGFs:

The surface area for the SGFs was calculated to be 839 $m^2 \cdot g^{-1}$ using the methylene blue adsorption method. Methylene blue is a common dye probe used to determine the surface area of graphitic materials, with each molecule of adsorbed methylene blue representing 1.35 nm^2 of surface area. [20-22] The surface area was calculated by adding a known mass of SGFs into a standard concentration of methylene blue in de-ionic water. SGFs were stirred in the methylene blue solution continuously at a rate of 1800 rpm for a total of 24 hours to reach maximum adsorption. The mixture was then allowed to settle and further centrifuged to remove any suspended material. The methylene blue concentration was determined by analyzing the supernatant through UV-visible spectroscopy at a wavelength of 664 nm and compared to the initial standard concentration of methylene blue prior to interacting with SGFs. Besides, the surface area for the PGFs was calculated to be 49 $m^2 \cdot g^{-1}$ by using the similar process.

Calculations methods:

The capacitance of the micro-SC cell derived from galvanostatic discharge curves was calculated based on the following equation: $C_{cell} = I \cdot \Delta t / \Delta E$, where I is the discharge current, Δt is the time for a full discharge and ΔE represents the potential change after a full discharge.

The specific capacitance of the active material in one single electrode was calculated based on the following equation: $C_X = 2 C_{cell} / X$, where X is the area (cm^2) or volume (cm^3) or the length (cm) of one single fiber electrode.

The energy density (E_X) and power density (P_X) of one device depicted in the

Ragone plots were calculated by using the equations:

$$E_X = (1/8) \times C_X \cdot \Delta E^2$$

$$P_X = E_X \times 3600 / \Delta t$$

where $_X$ represents the area (cm^2) or volume (cm^3), ΔE is the potential change after a full discharge, and Δt is the time for a full discharge.

Supporting References

[1] L. Viet Thong, H. Kim, A. Ghosh, J. Kim, J. Chang, V. Quoc An, P. Duy Tho, J.-H. Lee, S.-W. Kim, Y. H. Lee, Acs Nano 2013, 7, 5940.

[2] X. Chen, L. Qiu, J. Ren, G. Guan, H. Lin, Z. Zhang, P. Chen, Y. Wang, H. Peng, Advanced Materials 2013, 25, 6436.

[3] J. Ren, W. Bai, G. Guan, Y. Zhang, H. Peng, Advanced Materials 2013, 25, 5965.

[4] J. Ren, L. Li, C. Chen, X. Chen, Z. Cai, L. Qiu, Y. Wang, X. Zhu, H. Peng, Advanced Materials 2013, 25, 1155.

[5] K. Wang, Q. Meng, Y. Zhang, Z. Wei, M. Miao, Advanced Materials 2013, 25, 1494.

[6] J. A. Lee, M. K. Shin, S. H. Kim, H. U. Cho, G. M. Spinks, G. G. Wallace, M. D. Lima, X. Lepro, M. E. Kozlov, R. H. Baughman, S. J. Kim, Nature Communications 2013, 4,1970.

[7] Y. Meng, Y. Zhao, C. Hu, H. Cheng, Y. Hu, Z. Zhang, G. Shi, L. Qu, Advanced Materials 2013, 25, 2326.

[8] Y. Li, K. Sheng, W. Yuan, G. Shi, Chemical Communications 2013, 49, 291.

[9] Y. Fu, X. Cai, H. Wu, Z. Lv, S. Hou, M. Peng, X. Yu, D. Zou, Advanced Materials 2012, 24, 5713.

[10] X. Xiao, T. Li, P. Yang, Y. Gao, H. Jin, W. Ni, W. Zhan, X. Zhang, Y. Cao, J. Zhong, L. Gong, W.-C. Yen, W. Mai, J. Chen, K. Huo, Y.-L. Chueh, Z. L. Wang, J. Zhou, Acs Nano 2012, 6, 9200.

[11] J. Bae, M. K. Song, Y. J. Park, J. M. Kim, M. Liu, Z. L. Wang, Angewandte Chemie-International Edition 2011, 50, 1683.

[12] Y. Fu, H. Wu, S. Ye, X. Cai, X. Yu, S. Hou, H. Kafafy, D. Zou, Energy & Environmental Science 2013, 6, 805.

[13] W. Zhou, K. Zhou, X. Liu, R. Hu, H. Liu, S. Chen, Journal of Materials Chemistry A 2014, 2, 7250.

[14] D. Zhang, M. Miao, H. Niu, Z. Wei, Acs Nano 2014, 8, 4571.

[15] H. Sun, X. You, J. Deng, X. Chen, Z. Yang, J. Ren, H. Peng, Advanced Materials 2014, 26, 2868.

[16] C. Qing, M. Yuning, H. Chuangang, Z. Yang, S. Huibo, C. Nan, Q. Liangti, Journal of Power Sources 2014, 247, 32.

[17] K. Gopalsamy, Z. Xu, B. Zheng, T. Huang, L. Kou, X. Zhao, C. Gao, Nanoscale 2014, 6, 8595.

[18] M. F. El-Kady, R. B. Kaner, Nature Communications 2013, 4.

[19] L. Chen, Y. He, S. Chai, H. Qiang, F. Chen and Q. Fu, Nanoscale 2013, 5, 5809-5815.

[20] M. F. El-Kady, V. Strong, S. Dubin, R. B. Kaner, Science 2012, 335, 1326.

[21] Y. Xu, Z. Lin, X. Zhong, X. Huang, N. O. Weiss, Y. Huang, X. Duan, Nature Communications 2014, 5.

[22] R. S. Rubino, E. S. Takeuchi, Journal of Power Sources 1999, 81, 373.